Paranodal reorganization results in the depletion of transverse bands in the aged central nervous system

Mark N. Shepherd[a,b], **Anthony D. Pomicter**[a], **Cristine S. Velazco**[a], **Scott C. Henderson**[a], and **Jeffrey L. Dupree**[a,*]

[a]Department of Anatomy and Neurobiology, Virginia Commonwealth University, Richmond, VA, USA 23298

[b]MD Biosciences, 2575 University Avenue W. Suite 100 St Paul, MN, USA 55114 (present address)

Abstract

Paranodal axo-glial junctional complexes anchor the myelin sheath to the axon and breakdown of these complexes presumably facilitates demyelination. Myelin deterioration is also prominent in the aging central nervous system (CNS); however, the stability of the paranodal complexes in the aged CNS has not been examined. Here, we show that transverse bands, prominent components of paranodal junctions, are significantly reduced in the aged CNS; however, the number of paired clusters of both myelin and axonal paranodal proteins is not altered. Ultrastructural analyses also reveal that thicker myelin sheaths display a "piling" of paranodal loops, the cytoplasm-containing sacs that demarcate the paranode. Loops involved in piling are observed throughout the paranode and are not limited to loops positioned in either the nodal- or juxtanodal-most regions. Here, we propose that as myelination continues, previously anchored loops lose their transverse bands and recede away from the axolemma. Newly juxtaposed loops then lose their transverse bands, move laterally to fill in the gap left by the receded loops and finally reform their transverse bands. This paranodal reorganization results in conservation of paranodal length, which may be important in maintaining ion channel spacing and axonal function. Furthermore, we propose that transverse band reformation is less efficient in the aged CNS, resulting in the significant reduction of these junctional components. Although demyelination was not observed, we propose that loss of transverse bands facilitates myelin degeneration and may predispose the aged CNS to a poorer prognosis following a secondary insult.

Keywords

Myelin; Paranode; Transverse bands; Paranodal loops; Caspr; Neurofascin 155; Contactin; Voltage-gated sodium channel 1.6; Voltage-gated potassium channel 1.2

1. Introduction

The myelin sheath is tightly anchored to the axolemma by junctional complexes located in the paranode (Peters et al., 1991). These junctions are, at least in part, composed of the myelin protein neurofascin 155 and the axonal proteins contactin and Caspr (Bhat et al.,

*Corresponding author. Tel: +1-804 828 9536; fax: +1-804 828 9477. jldupree@vcu.edu (J.L. Dupree).

Disclosure statement
There are no potential or actual conflicts of interests on behalf of any of the authors.

2001; Bonnon et al., 2007; Boyle et al., 2001; Charles et al., 2002; Einheber et al., 1997; Gollan et al., 2002; Horresh et al., 2010; Rios et al., 2000; Schafer et al., 2004; Tait et al., 2000; Thaxton et al., 2010). Prominent components of these junctions are the regularly arrayed electron densities, known as transverse bands that bridge the space between the paranodal loops of the myelin sheath and the axolemma (Marcus et al., 2002; Peters et al., 1991; Tao-Cheng and Rosenbluth, 1983). In mice that lack functional neurofascin 155 (Pillai et al., 2009; Sherman et al., 2005; Thaxton et al., 2010; Zonta et al., 2008), contactin (Boyle et al., 2001) or Caspr (Bhat et al., 2001), transverse bands do not properly form and paranode structure and stability are compromised. Additionally, when these proteins are expressed but fail to cluster, transverse band formation is compromised, paranodal structure deteriorates and demyelination ensues (Coetzee et al., 1998; Dupree et al., 1998; Honke et al., 2002; Marcus et al., 2006).

In multiple sclerosis, the most common human demyelinating disease of the central nervous system (CNS), the distribution and expression of Caspr (Wolswijk and Balesar, 2003) and neurofascin 155 (Howell et al., 2006; Pomicter et al., 2010) are altered and these molecular changes are accompanied by the apparent loss of transverse bands and eversion of the paranodal loops (Suzuki et al., 1969). Importantly, these molecular and structural alterations, reminiscent of the genetically engineered mutant mice, precede myelin loss consistent with the possibility that these changes are suggestive of impending myelin degeneration.

In addition to being a consequence of genetic manipulation and disease, demyelination is also a prominent feature of normal aging of both the peripheral and the central nervous systems in a variety of species, including rodents, monkeys and humans (Bennett et al., 2010; Kochunov et al., 2009; Luebke et al., 2010; Peters and Sethares, 2002; Peters et al., 2001; Peters, 2009; Robertson et al., 1993; Sandell and Peters, 2003; Zhang et al., 2008). To determine whether age-related demyelination is also associated with paranodal deterioration, we analyzed the integrity of the CNS paranodal axo-glial junctions in mice ranging between 1 and 22 months of age. Our quantitative ultrastructural analyses provide the first evidence that transverse bands are compromised with age as a significant number of paranodes in aged animals lack a full complement of these structures; however, none of the paranodes completely lacks transverse bands. Correspondingly, the number of paranodal clusters of either Caspr or neurofascin 155 is not significantly reduced. Although we found no evidence that the paranodal loops separate or abnormally turn away from the axolemma, the loops frequently did not contact the axonal membrane. Moreover, we report that the loss of axonal contact is not an age-related event but results from an increase in myelin thickness and subsequent paranodal reorganization. Based on our findings, we propose that paranodal reorganization occurs at all ages, is essential for maintaining a conserved paranodal length and requires temporary breakdown of transverse bands. In adolescent (15 days and 1 month) and adult (8 and 12 months) mice, transverse bands are reformed rapidly; in contrast, in aged (17 and 22 months) mice transverse bands are not reformed as efficiently resulting in a cumulative loss of these junctional components. These findings are significant as the reduction of transverse bands may provide an additional confounding factor in clinical prognoses of aged individuals following injury or during disease processes.

2. Methods

2.1. Animals

C57/black6 mice were bred, housed and aged (up to 22 months) in the Virginia Commonwealth University Division of Animal Resources vivarium. Twenty-two months was chosen as the terminal age as this was the oldest survival age that the mice would consistently achieve. In addition, aged (17 and 22 months) C57/black6 mice were also generously provided by the National Institute of Aging (exception approval # 4M09JD1).

All procedures were conducted in accordance with the Virginia Commonwealth University Animal Care and Use Committee.

2.2. Electron microscopic analyses

Spinal cord samples spanning cervical regions C4-C6 from 15 day, 1 month, 8 month, 12 month, 17 month and 22-month-old mice were prepared for electron microscopic examination and analyzed on a JEOL JEM1230 transmission electron microscope equipped with a Gatan Ultrascan 4,000SP CCD camera as previously described (Dupree et al., 1998; Shroff et al., 2009).

2.3. Quantification of transverse band integrity and qualitative assessment of paranodal loop organization

For each mouse aged 1 month through 22 months, one ultrathin section (90 nm) cut from a longitudinally oriented tissue sample with an approximate area of 2.25 mm^2 (1.5 mm on a side) was examined. Every nodal region flanked by two completely visible paranodal regions was imaged at a magnification of 3,000× and 25,000× resulting in a total of 278 paranode/node/paranode (PNP) domains. The number of mice analyzed and the number of PNP domains imaged per age were 1 month (six mice; n = 60 PNP domains), 8 months (six; 35), 12 months (three; 57), 17 months (three; 50) and 22 months (five; 76). Quantitative analysis of transverse band integrity and loop organization were not conducted on 15-day-old mice as we have previously reported that transverse bands and the paranode are not fully formed until the third week of life (Marcus et al., 2002). Although not used in the transverse band integrity study, PNP domains imaged from 15-day-old mice were used to determine whether lateral loop "piling" was a feature of age. For this analysis, a total of 40 PNP domains were collected from four mice.

Of the 278 nodal/paranodal regions collected from the 1-to 22-month-old mice, only 157 of the PNP domains were used for quantitation of transverse band integrity as each PNP domain was required to meet several criteria: 1) juxtaparanodal regions, identified by the presence of compact myelin, had to be visible; 2) periaxonal space, axolemma and membrane of the paranodal loops for a minimum of four adjacent loops had to be resolved; and 3) the four adjacent loops had to be positioned in the central portion of the paranode as transverse bands are frequently not formed between the axolemma and the paranodal loops most nodally (unpublished observation) and juxtaparanodally positioned (Allt, 1969; Berthold, 1968). The central portion of the paranode was defined as the paranode between the first nodally positioned loop with transverse bands and the first juxtaparanodally positioned paranodal loop with transverse bands. If a central region of the paranode could not be identified, the paranode was deemed unsuitable for further analysis. The number of PNP domains deemed suitable for the transverse band integrity study per age group was 1 month (n = 34), 8 months (n = 27), 12 months (n = 31), 17 months (n = 32) and 22 months (n = 33).

Transverse band integrity was quantitatively analyzed for appropriate transverse band spacing. As transverse bands are ~15 nm wide and are ≤ 25 nm apart, measured center to center of adjacent bands (Peters et al., 1991; Schnapp et al., 1976), a gap of greater than 35 nm indicates the absence of a transverse band. For all analyses in this study, a minimum gap of 45 nm was required to conclude the absence of a transverse band. Gaps between adjacent transverse bands of juxtaposed loops were variable. Thus, gap spacing analyses did not include the regions between adjacent paranodal loops. Therefore, variable spacing between loops would not falsely implicate the absence of a transverse band. The percentage of paranodal regions that displayed missing transverse band(s) was calculated per mouse at

each age. Data were analyzed with an ANOVA followed by a posthoc Tukey–Kramer (SPSS 18 software).

In addition to the quantitative transverse band analysis, the periaxonal space of all 278 PNP domains was qualitatively assessed for gross changes in width and/or focal irregularities, such as out pocketing or indentations and paranodal loops were analyzed for orientation (eversion vs inversion), organization (ordered vs disordered alignment), and axolemmal contact. For each PNP domain, myelin thickness of the compacted myelin immediately outside of the paranode was determined using ImageJ (rsb.info. nih.gov/ij/).

2.4. Immunocytochemical analyses

One month (n = 3 mice), 8 months (n = 4), 12 months (n = 3), 17 months (n = 3), and 22 months (n = 4) old mice were perfused with 4% formaldehyde in Millonigs buffer. Cervical spinal cord samples were cryosectioned, immunolabeled with the appropriate primary and fluorescently labeled secondary antibodies, and imaged using a Leica TCS-SP2 AOBS laser scanning confocal microscope (Leica Microsystems, Inc., Exton, PA) as previously described (Dupree et al., 1999; Dupree et al., 2004; Pomicter et al., 2010; Shroff et al., 2009). Two spinal cord samples were collected per animal; one sample was embedded for longitudinal analysis while the second sample was used for transverse analysis. Longitudinally sectioned spinal cord samples were single immunolabeled for Caspr and double immunolabeled using the following combinations: voltage gated potassium channel ($K_v1.2$) and Caspr; $K_v1.2$ and pan neurofascin; $K_v1.2$ and contactin; and Caspr and voltage gated sodium channel ($Na_v1.6$). The cross sectioned samples were single labeled for phosphorylated neurofilament.

2.5. Antibodies

The Caspr (guinea-pig; 1:1,000) and the rat pan neurofascin (1:1,000) antibodies were generous gifts from Dr Manzoor Bhat (University of North Carolina at Chapel Hill; Pillai et al., 2007; Pillai et al., 2009). The rabbit contactin antibody (1:200) was kindly provided by Dr Jim Salzer (New York University). The mouse $K_v1.2$ (clone K14/16, 1: 500) and $Na_v1.6$ (clone K87A/10, 1:500) antibodies were purchased from the University of California, Davis NINDS/ NIMH NeuroMab Facility. The neurofilament antibody (SMI 31; 1:1,000) was purchased from Sternberger Monoclonal, Inc. (Baltimore, MD). Fluorescently labeled secondary antibodies were purchased from Vector Laboratories, Inc. (1:200; Burlingame, CA) and Invitrogen (1:500; Carlsbad, CA). To confirm specificity of the labels, no-primary and species-appropriate normal sera controls followed by fluorescently conjugated secondary antibodies were conducted in parallel with the immunolabeling studies (not shown).

2.6. Qualitative and quantitative assessment of Caspr and neurofascin paranodal clustering

For qualitative assessment of paranodal and nodal protein clustering and for quantitative assessment of paranodal protein clustering, a minimum of six images per animal was collected. The caudal aspect of the cerebellum, which was left attached to the harvested spinal cord, was used to establish anterior/posterior and dorsal/ventral orientations. Images were collected only from the ventral column of the cervical spinal cord; the starting point for image collection was at the level of C1. All images were collected using a 63×/1.4NA PlanApo oil immersion objective lens. The magnification was increased by zooming in the scan by a factor of two. Using Nyquist sampling criteria for a Z-stack through a depth of 2 μm, images were collected with a pinhole setting of one Airy disk unit and quantified using the projected average intensity image. A microscopic field was 119 × 119 μm. The scan resolution was set at 2,048 × 2,048 pixels. The detector windows settings used for collecting

emission for the Alexa Fluor 488 or FITC and Alexa Fluor 594 were 510–540 nm and 620–660 nm, respectively.

For quantitative assessment, all double immunolabeled images were studied for overlapping fluorescent signals, which has been previously used to infer a "mixing" of juxtaparanodal/paranodal and paranodal/nodal domains (Dupree et al., 1999). For quantitative analysis, the relative number of Caspr+ paired clusters and neurofascin+ clusters was determined. A Caspr+ paranodal cluster pair was identified as two adjacent accumulations separated by an approximately 1 μm, unlabeled region corresponding to the node of Ranvier. As the neurofascin antibody immunoreacts with both neurofascin 155, the oligodendrocytic form, and neurofascin 186, the neuronal form, we used the criteria previously established in the laboratory for quantitation of paranodal neurofascin clusters (see Pomicter et al., 2010). Adobe Photoshop CS3 software (Adobe, Inc, San Jose, CA) was used to confirm the area of the image field and to determine the number of Caspr+ and neurofascin 155+ paranodal clusters per microscopic field.

2.7. Standardizing Caspr and neurofascin paranodal clustering counts based on axonal density

Transversely oriented frozen spinal cord sections from the cervical region were immunolabeled with SMI 31, an antibody directed against the phosphorylated neurofilament high and middle molecular weight subunits. To quantify axonal density, a minimum of four images per spinal cord was collected using the Leica confocal microscope with the same settings described above with the exception that the images resulted from a single optical slice with an image depth of 0.24 μm. The number of axons per image field was calculated based on the intensity of labeling using IPLab (BD Biosciences, Rockville, MD). An optimal segmentation threshold was determined for each age group without saturation so that closely apposed axons were not artificially grouped.

3. Results

3.1. Transverse bands are significantly reduced in the aged CNS

To quantitatively assess paranodal integrity in the aged CNS, we determined the percentage of paranodes that lacked the full complement of transverse bands in mice 1, 8, 12, 17 and 22 months of age. A full complement of transverse bands was indicated by the absence of gaps greater than 35 nm (see Materials and methods).

As shown in Figure 1A, transverse bands are electron densities that span the periaxonal space (Peters et al., 1991). Consistent with the work of Sugiyama et al. (2002), all paranodes, regardless of the age of the animal, displayed transverse bands. However, the full complement of transverse bands was not always observed (Figure 1B, C and D). In mice 1, 8 and 12 months of age, the full complement of transverse bands was observed in approximately 90% of the PNP domains (94.5 ± 6.1%, 91.8 ± 6.4%, 86.9 ± 12.5%, respectively). At these ages, transverse bands were visible with clearly defined borders revealing no signs of deterioration. At 17 and 22 months, however, the full complement of transverse bands was observed in only about half of the paranodes (50 ± 0%, 36.1 ± 13.3%, respectively) which are significant reductions compared with 1, 8 and 12 months of age (Figure 1E, $p < 0.05$ via the Tukey–Kramer method). Additionally, at these older ages, edges of transverse bands were occasionally poorly defined (Figure 1C, black arrow heads).

3.2. Distribution of paranodal proteins is modestly altered in the aged CNS

Since the ultrastructural analysis revealed a significant deficiency in the number of transverse bands in the aged CNS, we proposed that paranodal distribution of Caspr,

contactin and neurofascin 155 would be progressively altered with age. As shown in Figure 2A, paired clusters of Caspr were observed in the ventral column of the spinal cord from mice of all ages. In 1-month-old mice the paired clusters revealed a definitive delineation between the paranode and the juxtaparanode and between the paranode and the presumptive node of Ranvier. Note, at this age, no Caspr immunolabeling was observed in nodal, juxtaparanodal or internodal regions (Figure 2A). Although immunolabeling for Caspr was never observed in the node at any age, aged mice occasionally displayed low intensity Caspr labeling in the juxtaparanode and internode (Figure 2F). Additionally, a line of immunoreactivity against the Caspr antibody, consistent with previous reports of Caspr labeling of the mesaxon (Altevogt et al., 2002; Arroyo et al., 1999; Arroyo et al., 2001; Melendez-Vasquez et al., 2001; Menegoz et al., 1997), was not observed at 1 month of age but became more prominent with age (Figure 2A–E). Similar to Caspr, contactin (Figure 2G–K) and neurofascin 155 (Figure 2L–P) labeling was also observed in all paranodes regardless of the age of the animal. Note in Figure 2N a line of immunoreactivity against the neurofascin antibody that is reminiscent of the presumed Caspr labeled mesaxon observed in Figure 2B–D.

Migration of juxtaparanodal potassium channels into the paranode has been reported as an early indicator of compromised paranodal structure (Dupree et al., 1999; Rasband, 2004). In contrast to a previous study with aged monkeys and rats (Hinman et al., 2006), potassium channel localization was not altered in the aged mice (Figure 2). $Na_v1.6$ immunolabeling also revealed no abnormal distribution for nodally positioned voltage gated sodium channels (Figure 3) consistent with a previous report (Hinman et al., 2006).

3.3. The number of paranodal clusters of either Caspr or neurofascin 155 is not significantly reduced in the aged CNS

To quantitatively assess the maintenance of paranodal protein domains, we counted the number of paired paranodal clusters of Caspr and neurofascin 155 in mice 1, 8 and 22 months of age. To standardize cluster counts for age-related differences due to variable susceptibility to fixation artifact (Haug, 1986), increased axonal caliber (Marcus et al., 2006) and thicker myelin sheaths (Peters et al., 2001), relative axonal densities were determined using neurofilament-immunolabeled transverse cervical spinal cord sections (data not shown). Upon correcting for axonal density, the relative number of Caspr clusters per area at 1, 8, and 22 months of age was 17.5 ± 1.3, 17.4 ± 6.0 and 17.1 ± 4.1, respectively and the number of neurofascin paranodal clusters was 14.0 ± 0.4, 9.3 ± 4.9 and 11.1 ± 6.9, respectively. No statistical difference was observed in the number of paranodal clusters of either Caspr or neurofascin 155 among these ages indicating no loss of paranodal protein domains with age.

3.4. Paranodal loops frequently "pile up" and do not contact the axolemma

In addition to analyzing transverse band integrity, we also assessed paranode organization since paranodal loop orientation and position with respect to the axolemma are indicators of paranode stability (Bhat et al., 2001; Boyle et al., 2001; Dupree et al., 1998; Honke et al., 2002; Marcus et al., 2000; Pillai et al., 2009; Sherman et al., 2005; Thaxton et al., 2010). Although the percentage of paranodes with the full complement of transverse bands was significantly reduced at both 17 and 22 months of age, neither noticeable changes in the width of the periaxonal space nor indicators of demyelination, such as the presence of large (diameter of $\geq 1\ \mu m$) unmyelinated axons or myelin debris, was observed. Paranodal loops were appropriately arranged with the first loop maintaining the most distal position from the node and everted paranodal loops were confined to the region immediately adjacent to the node. Such everted loops were observed at all ages with no increased frequency with age. Similar findings have been previously reported for peripheral nervous system (PNS)

paranodes (Yamamoto et al., 1996) indicating that eversion of paranodal loops closest to the node is a normal event in both the PNS and the CNS.

Although everted paranodal loops were not observed in the central portion of the paranodes, paranodal loops frequently did not make contact with the axolemma (Figure 4). This observation is consistent with previous studies that have reported a "piling up" of paranodal loops in the PNS (Berthold, 1978; Bertram and Schröder, 1993) and the CNS (Hinman et al., 2006). Hinman et al. (2006) reported that piling up of paranodal loops occurred more frequently in paranodes of thick myelin sheaths from older animals. Based on this observation, it is possible that paranodal loop piling is related to age or myelin thickness or both. To distinguish among these possibilities, we determined the frequency of piled paranodal loops at each age. We observed piled paranodal loops in approximately half of all paranodes at all ages (26 of 60 paranodes at 1 month; 22 of 35 paranodes at 8 months, 30 of 57 paranodes at 12 months, 30 of 50 paranodes at 17 months and 38 of 76 paranodes at 22 months; Figure 4D). To further determine whether piling of paranodal loops is related to aging, we also determined the frequency of piling paranodal loops in immature mice. At 15 days of age, 14 of 40 paranodes revealed piling of paranodal loops. Because the frequency of piling of paranodal loops is approximately the same for mice between the ages of 1 and 22 months and because piling is also prevalent even in the immature CNS, these findings indicate that piling of paranodal loops occurs independent of aging.

3.5. Piling of paranodal loops commonly associates with thick myelin sheaths

To determine whether piling of paranodal loops is related to the extent of myelination, we measured the thickness of the compact myelin immediately adjacent to each paranode observed. First, myelin thickness increased significantly between 1 and 8 months of age ($0.214 \pm 0.108\ \mu$m at 1 month vs $0.386 \pm 0.220\ \mu$m at 8 months; $p = 0.003$). A modest increase was again observed between 8 and 12 months of age (compare $0.386 \pm 0.220\ \mu$m at 8 months vs $0.423 \pm 0.345\ \mu$m at 12 months) which was accompanied by an increase in variability in sheath thickness as indicated by the larger standard deviation. Average myelin sheath thickness at 17 and 22 months of age were $0.466 \pm 0.237\ \mu$m, and $0.430 \pm 0.289\ \mu$m, respectively.

Although our data do not suggest a correlation between paranodal loop piling and age, our findings indicate a strong correlation between myelin thickness and paranodal loop piling. As shown in Figure 4D, only 10% (15 of 150) of the paranodes formed by myelin sheaths < $0.25\ \mu$m thick, regardless of age, revealed loop piling. In contrast, 87% (146 of 168) of the paranodes formed from myelin sheaths $\geq 0.25\ \mu$m contained piled paranodal loops indicating a strong correlation between paranodal loop piling and myelin thickness regardless of age.

3.6. Paranode length is conserved in the CNS

In 1993 Bertram and Schröder reported that paranodal length in the PNS is conserved and that length conservation is regulated by paranodal loop piling. Consistent with the PNS, our data indicate that paranodal length is also conserved in the CNS. As shown in Figure 5A, no significant difference in paranodal length was observed among any of the ages with mean paranodal lengths ranging between 2.7 and 3.3 μm ($3.3 \pm 1.1\ \mu$m at 15 days, $3.0 \pm 0.9\ \mu$m at 1 month; $2.7 \pm 0.7\ \mu$m at 8 months; $2.9 \pm 0.9\ \mu$m at 12 months; $3.1 \pm 1.1\ \mu$m at 17 months and $2.8 \pm 0.9\ \mu$m at 22 months). Plotting paranodal length against myelin thickness (Figure 5B) demonstrates that longer paranodes generally accompany thicker myelin sheaths; however, the scatter plot indicates that the rate of paranodal lengthening is not maintained as myelin thickness increases. This difference in rate lengthening is demonstrated by graphing paranodes from myelin sheaths thinner than 0.25 μm separately (Figure 5C) from paranodes

from myelin sheaths ≥ 0.25 μm (Figure 5D). (0.25 μm was used to divide the two groups as this was the threshold for paranodal loop piling (Figure 4D). The apparent difference in rate lengthening was confirmed by calculating the slopes of the best fit lines for myelin sheaths < 0.25 μm and for myelin sheaths ≥ 0.25 μm. Based on slope calculations, the rate of paranodal lengthening for myelin sheaths < 0.25 μm is 4.45 μm of paranodal lengthening per 1 μm of myelin thickness while the rate of paranodal lengthening for myelin sheaths ≥ 0.25 μm is 1.5 μm of paranodal length per 1 μm of myelin thickness. Thus the rate of paranodal lengthening in thinly myelinated axons is ~3 times greater than the rate of paranodal lengthening in heavily myelinated axons.

Although paranodal loop piling was observed more frequently, "thinning" of paranodal loops was also observed. As shown in Figure 4C, the shape of paranodal loops occasionally became elongated and the portion of the loop designated to contact the axolemma was substantially thinner. Thus, in addition to paranodal loop piling, paranodal loop thinning also contributes to paranodal length conservation.

To better understand the event of paranodal loop piling, we analyzed the paranodes to determine whether loops at a specific location along the paranodal domain had a greater propensity to participate in piling. Most nodally positioned loops frequently did not contact the axolemma and appeared piled; however, loops positioned in the central portion of the paranodal domain also participated in loop piling (Figure 6). Additionally, as shown in Figure 6B, adjacent lateral loops, positioned "beneath" piled loops, were often separated by an enlarged gap and lacked transverse bands.

4. Discussion

In this study, we provide the first evidence that in the CNS transverse bands are lost with age. Although transverse bands are reduced, we observed no evidence of further paranodal deterioration, such as paranodal loop eversion, expanded periaxonal space, altered distribution of the proteins implicated in transverse band formation or improper localization of either K_v or Na_v ion channels. Importantly, no paranode displayed a complete absence of transverse bands. We also present the first evidence that CNS paranodal length is conserved and we propose that length conservation is achieved, at least in part, by paranodal loop piling. Although CNS paranodal loop piling has previously been reported, we provide strong evidence that piling is independent of age but is correlative to myelin sheath thickness. Taken together, our findings reveal an age-dependent alteration in the structure of paranodal axo-glial junctions and demonstrate that the paranode is a dynamic entity requiring reorganization throughout life.

4.1. Are transverse bands a requirement for paranodal integrity?

The precise role of transverse bands remains unclear; however, these "bands" appear to anchor the myelin sheath to the axon thus stabilizing the axo-glial interface. Although implied by the name, transverse bands are not columns that traverse the periaxonal space but are the two-dimensional representation observed by electron microscopy resulting from a spiraling interface between the myelin paranodal loops and axolemma (Hirano and Dembitzer, 1969). Thus, the absence of a transverse band results from a focal disruption of the paranodal contact interface between the myelin sheath and the axon. Such a limited disruption, as evidenced by the absence of one or a few transverse bands, may be insufficient for gross paranodal deterioration. However, even the partial loss of the full complement of transverse bands may result in a weaker anchorage of the myelin sheath to the axon making the CNS more vulnerable to a secondary insult. This intriguing possibility is consistent with poorer prognoses for late onset MS patients (reviewed in Bergamaschi, 2007) and elderly victims of CNS injury (Wasserman and Schlichter, 2008).

Gross maintenance of paranodal structure in the presence of compromised transverse band integrity is consistent with previous findings of Rosenbluth et al. (2003) that paranodal junctions are formed only in part by the transverse bands. For example, paranodal regions are established before the formation of transverse bands (Marcus et al., 2002; Tao-Cheng and Rosenbluth, 1983) and mice that are incapable of normal transverse band formation establish regions that resemble paranodes with regard to both structure and molecular composition and form prevalent axolemmal invaginations (Rosenbluth et al., 2003). Consistent with the observation that the paranode formation occurs without, or before, transverse band formation, the same mechanisms that regulate initial synthesis may also act to maintain the region independent of transverse bands.

4.2. Why are transverse bands lost?

The present study is not the first to report missing transverse bands. Berthold (1968) reported that the innermost paranodal loops frequently lack transverse bands, which may facilitate continued myelin formation. Furthermore, Tao-Cheng and Rosenbluth (1982) reported the absence of transverse bands during myelin development while Allt (1969) reported a similar observation during remyelination. In addition to myelin formation, missing transverse bands have also been reported during myelin loss, including demyelination associated with pharmacological toxicity (Hirano and Zimmerman, 1971), multiple sclerosis (Suzuki et al., 1969) and experimental allergic neuritis (Allt, 1975). The absence or reduction of transverse bands during myelin loss may facilitate myelin degeneration by weakening the myelin-axon anchorage. Here, we provide the first evidence of the reduction of transverse bands independent of early development or myelin deterioration. It should be noted, however, that numerous studies have reported age-related CNS white matter decrease, compromised myelin integrity and demyelination (Bartzokis et al., 2003; Bennett et al., 2010; Dickstein et al., 2007; Duce et al., 2008; Guttmann et al., 1998; Kochunov et al., 2009; Luebke et al., 2010; Peters and Sethares, 2002; Peters et al., 2001; Peters, 2009; Robertson et al., 1993; Sandell and Peters, 2003; Zhang et al., 2008). Although we observed no signs of demyelination, the possibility remains that myelin deterioration may have been in early stages but not yet detected by ultrastructural observation.

Another explanation for the age-related reduction of transverse bands is an impaired capacity to replace the bands following paranode reorganization, which is required for conservation of paranodal length. In order for paranodal loop piling to occur, Bertram and Schröder (1993) postulated that in the PNS transverse bands of anchored paranodal loops would degenerate to facilitate loop retraction. Subsequently, adjacent loops would also lose their transverse bands to reposition to fill any gap created by the retracted loop. Upon establishing their new position along the axonal membrane, these loops would then reform their transverse bands. We propose that a similar course of events occurs in the CNS at all ages, which would explain the absence of the full complement of transverse bands at all ages studied. Consistent with this idea, two loops indicated in Figure 6A are positioned above the axolemma and below these loops is an enlarged gap between adjacent lateral loops. This image is consistent with the idea that loops, initially anchored to the axolemma by transverse bands, lose this anchorage and retract. Subsequently, the remaining adjacent loops lose their transverse bands, and reposition to fill the existing gap. Upon repositioning, these newly adjacent loops reform their transverse bands; however, in the younger ages, transverse band reformation occurs efficiently while in the aged individuals, band reformation is retarded or inhibited. The mechanism responsible for this inhibition of band reformation remains to be determined.

4.3. How and why is paranodal length conserved?

Because each wrap of myelin corresponds to the formation of an additional paranodal loop, the paranodal length should directly correlate to the number of myelin lamellae. From the findings of the current study, paranodal length is conserved at approximately 3 μm and at the point when myelin thickness reaches 0.25 μm, paranodal loops begin to pile on top of each other. Similarly, a previous study reported that as PNS myelin sheaths increase in thickness, paranodal length does not reveal a corresponding elongation although larger axons typically displayed longer paranodes (Bertram and Schröder, 1993). In contrast, Hinman et al. (2006) observed a direct correlation between the increase in CNS myelin thickness and paranodal lengthening suggesting that paranodal growth is differentially regulated by the PNS compared with the CNS. In the latter study, Hinman et al. (2006) analyzed myelinated axons from brain area 17, a region that contains relatively small axons with correspondingly thin myelin sheaths (≤ 20 lamellae or myelin sheaths ≤ 0.2 μm thick). Bertram and Schröder (1993) analyzed myelinated axons from the sural nerve with myelin sheaths up to 1.5 μm thick. In these heavily myelinated axons, newly formed paranodal loops began to "pile up" and paranodal loops were attenuated. The results from this PNS study parallel the findings of the current study with heavily myelinated axons displaying piled and narrowed paranodal loops. We postulate that the discrepancy between the current work and the previous CNS report results from the thickness of the myelin sheaths analyzed. The previous study focused on myelinated sheaths that were too thin to demonstrate the retarded lengthening that is observed in thick sheaths. Taken together, our current findings, combined with the findings of Bertram and Schröder (1993), indicate that paranode length is conserved in both the PNS and the CNS and that the two systems employ similar coping mechanisms.

It remains to be determined, however, why paranodal length is conserved. As axonal constriction at the nodal and paranodal regions in both the PNS (Swärd et al., 1995) and the CNS (Rydmark, 1981) may impede axonal transport (Armstrong et al., 1987), Cooper and Smith (1974) postulated that a reduced length of constriction might facilitate the movement of vesicles and organelles along the axon. Alternatively, we propose that the conserved distance between the juxtaparanodal K_v channels and the nodal Na_v channels results in efficient axonal function. Whereas the Na_v channels depolarize the axonal membrane to propagate an action potential, the K_v channels are thought to repolarize the axonal membrane to reduce latency or to maintain an internodal resting potential (Chiu and Ritchie, 1981; Ritchie and Chiu, 1981; Vabnick et al., 1999). Thus, the nodal Na_v channels and the juxtaparanodal K_v channels act in opposition to each other. If these ion channel clusters are too close, they may inhibit each other's function; however, if the K_v channels are too far removed from the nodal region, then repolarization efficiency may be retarded. Ultimately, any abnormal localization of the Na_v channels or K_v channels could be responsible for impaired neuronal conduction velocity.

Perhaps a less complicated explanation lies with the node of Ranvier. If paranode lengthening continues unbridled, then the node could be obscured by the encroaching paranodal loops. Although it is unclear what functional impairment would result from such encroachment, it is plausible to predict a dramatic alteration in ion channel spacing, density and function resulting in loss of or less efficient impulse propagation.

In conclusion, the findings from this study show that with advanced age the number of transverse bands is significantly reduced, but that this moderate loss of transverse bands does not grossly compromise paranodal structure. Moreover, we propose that this age-dependent loss of transverse bands results from less efficient paranodal reorganization, an event that occurs at all ages and is essential for maintaining an optimal paranodal length. Although the loss of transverse bands presented in this work does not correlate with gross loss of paranodal integrity, it remains to be determined whether this moderate alteration in

paranode structure results in functional impairment or predisposes the CNS to poorer prognoses following a secondary insult.

Acknowledgments

References

Allt G. Repair of segmental demyelination in peripheral nerves: an electron microscope study. Brain. 1969; 92:639–646. [PubMed: 5806128]

Allt G. The node of Ranvier in experimental allergic neuritis: an electron microscope study. J Neurocytol. 1975; 4:63–76. [PubMed: 1113142]

Altevogt BM, Kleopa KA, Postma FR, Scherer SS, Paul DL. Connexin29 is uniquely distributed within myelinating glial cells of the central and peripheral nervous systems. J Neurosci. 2002; 22:6458–6470. [PubMed: 12151525]

Armstrong R, Toews AD, Morell P. Axonal transport through nodes of Ranvier. Brain Res. 1987; 412:196–199. [PubMed: 3607457]

Arroyo EJ, Xu YT, Zhou L, Messing A, Peles E, Chiu SY, Scherer SS. Myelinating Schwann cells determine the internodal localization of Kv1.1, Kv1.2, Kvbeta2, and Caspr. J Neurocytol. 1999; 28:333–347. [PubMed: 10739575]

Arroyo EJ, Xu T, Poliak S, Watson M, Peles E, Scherer SS. Internodal specializations of myelinated axons in the central nervous system. Cell Tissue Res. 2001; 305:53–66. [PubMed: 11512672]

Bartzokis G, Cummings JL, Sultzer D, Henderson VW, Nuechterlein KH, Mintz J. White matter structural integrity in healthy aging adults and patients with Alzheimer disease: a magnetic resonance imaging study. Arch Neurol. 2003; 60:393–398. [PubMed: 12633151]

Bennett IJ, Madden DJ, Vaidya CJ, Howard DV, Howard JH Jr. Age-related differences in multiple measures of white matter integrity: A diffusion tensor imaging study of healthy aging. Hum Brain Mapp. 2010; 31:378–390. [PubMed: 19662658]

Bergamaschi R. Prognostic factors in multiple sclerosis. Int Rev Neurobiol. 2007; 79:423–447. [PubMed: 17531853]

Berthold CH. Ultrastructure of postnatally developing feline peripheral nodes of Ranvier. Acta Soc Med Ups. 1968; 73:145–168. [PubMed: 5706386]

Bertram M, Schröder JM. Developmental changes at the node and paranode in human sural nerves: morphometric and fine-structural evaluation. Cell Tissue Res. 1993; 273:499–509. [PubMed: 8402830]

Bhat MA, Rios JC, Lu Y, Garcia-Fresco GP, Ching W, St Martin M, Li J, Einheber S, Chesler M, Rosenbluth J, Salzer JL, Bellen HJ. Axon-glia interactions and the domain organization of myelinated axons requires neurexinIV/Caspr/Paranodin. Neuron. 2001; 30(2):369–83. [PubMed: 11395000]

Bonnon C, Bel C, Goutebroze L, Maigret B, Girault JA, Faivre-Sarrailh C. PGY repeats and N-glycans govern the trafficking of paranodin and its selective association with contactin and neurofascin-155. Mol Biol Cell. 2007; 18:229–241. [PubMed: 17093057]

Boyle ME, Berglund EO, Murai KK, Weber L, Peles E, Ranscht B. Contactin orchestrates assembly of the septate-like junctions at the paranode in myelinated peripheral nerve. Neuron. 2001; 30:385–397. [PubMed: 11395001]

Charles P, Tait S, Faivre-Sarrailh C, Barbin G, Gunn-Moore F, Denisenko-Nehrbass N, Guennoc AM, Girault JA, Brophy PJ, Lubetzki C. Neurofascin is a glial receptor for the paranodin/Caspr-

contactin axonal complex at the axoglial junction. Curr Biol. 2002; 12:217–220. [PubMed: 11839274]

Chiu SY, Ritchie JM. Evidence for the presence of potassium channels in the paranodal region of acutely demyelinated mammalian single nerve fibres. J Physiol. 1981; 313:415–437. [PubMed: 6268773]

Coetzee T, Dupree JL, Popko B. Demyelination and altered expression of myelin-associated glycoprotein isoforms in the central nervous system of galactolipid-deficient mice. J Neurosci Res. 1998; 54:613–622. [PubMed: 9843152]

Cooper PD, Smith RS. The movement of optically detectable organelles in myelinated axons of Xenopus laevis. J Physiol. 1974; 242:77–97. [PubMed: 4140230]

Dickstein DL, Kabaso D, Rocher AB, Luebke JI, Wearne SL, Hof PR. Changes in the structural complexity of the aged brain. Aging Cell. 2007; 6:275–284. [PubMed: 17465981]

Duce JA, Podvin S, Hollander W, Kipling D, Rosene DL, Abraham CR. Gene profile analysis implicates Klotho as an important contributor to aging changes in brain white matter of the rhesus monkey. Glia. 2008; 56:106–117. [PubMed: 17963266]

Dupree JL, Coetzee T, Blight A, Suzuki K, Popko B. Myelin galactolipids are essential for proper node of Ranvier formation in the CNS. J Neurosci. 1998; 18:1642–1649. [PubMed: 9464989]

Dupree JL, Girault JA, Popko B. Axo-glial interactions regulate the localization of axonal paranodal proteins. J Cell Biol. 1999; 147:1145–1152. [PubMed: 10601330]

Dupree JL, Mason JL, Marcus JR, Stull M, Levinson R, Matsushima GK, Popko B. Oligodendrocytes assist in the maintenance of sodium channel clusters independent of the myelin sheath. Neuron Glia Biol. 2004; 1:179–192. [PubMed: 18634596]

Einheber S, Zanazzi G, Ching W, Scherer S, Milner TA, Peles E, Salzer JL. The axonal membrane protein Caspr, a homologue of neurexin. IV, is a component of the septate-like paranodal junctions that assemble during myelination. J Cell Biol. 1997; 139:1495–1506. [PubMed: 9396755]

Gollan L, Sabanay H, Poliak S, Berglund EO, Ranscht B, Peles E. Retention of a cell adhesion complex at the paranodal junction required the cytoplasmic region of Caspr. J Cell Biol. 2002; 157:1247–1256. [PubMed: 12082082]

Guttmann CR, Jolesz FA, Kikinis R, Killiany RJ, Moss MB, Sandor T, Albert MS. White matter changes with normal aging. Neurology. 1998; 50:972–978. [PubMed: 9566381]

Haug H. History of neuromorphometry. J Neurosci Methods. 1986; 18:1–17. [PubMed: 3540464]

Hinman JD, Peters A, Cabral H, Rosene DL, Hollander W, Rasband MN, Abraham CR. Age-related molecular reorganization at the node of Ranvier. J Comp Neurol. 2006; 495:351–362. [PubMed: 16485288]

Hirano A, Dembitzer HM. The transverse bands as a means of access to the periaxonal space of the central myelinated nerve fiber. J Ultrastruct Res. 1969; 28:141–149. [PubMed: 5791690]

Hirano A, Zimmerman HM. Some new pathological findings in the central myelinated axon. J Neuropathol Exp Neurol. 1971; 30:325–336. [PubMed: 5567569]

Honke K, Hirahara Y, Dupree J, Suzuki K, Popko B, Fukushima K, Fukushima J, Nagasawa T, Yoshida N, Wada Y, Taniguchi N. Paranodal junction formation and spermatogenesis require sulfoglycolipids. Proc Natl Acad Sci U S A. 2002; 99:4227–4232. [PubMed: 11917099]

Horresh I, Bar V, Kissil JL, Peles E. Organization of myelinated axons by Caspr and Caspr2 requires the cytoskeletal adapter protein, p. 4, 1B. J Neurosci. 2010; 30(7):2,480–9. [PubMed: 20053882]

Howell OW, Palser A, Polito A, Melrose S, Zonta B, Scheiermann C, Vora AJ, Brophy PJ, Reynolds R. Disruption of neurofascin localization reveals early changes preceding demyelination and remyelination in multiple sclerosis. Brain. 2006; 129:3173–3185. [PubMed: 17041241]

Kochunov P, Ramage AE, Lancaster JL, Robin DA, Narayana S, Coyle T, Royall DR, Fox P. Loss of cerebral white matter structural integrity tracks the gray matter metabolic decline in normal aging. Neuroimage. 2009; 45:17–28. [PubMed: 19095067]

Luebke J, Barbas H, Peters A. Effects of normal aging on prefrontal area 46 in the rhesus monkey. Brain Res Rev Brain Res Rev. 2010; 62:212–232.

Marcus J, Dupree JL, Popko B. Effects of galactolipid elimination on oligodendrocyte development and myelination. Glia. 2000; 30:319–328. [PubMed: 10797612]

Marcus J, Dupree JL, Popko B. Myelin-associated glycoprotein and myelin galactolipids stabilize developing axo-glial interactions. J Cell Biol. 2002; 156:567–577. [PubMed: 11827985]

Marcus J, Honigbaum S, Shroff S, Honke K, Rosenbluth J, Dupree JL. Sulfatide is essential for the maintenance of CNS myelin and axon structure. Glia. 2006; 53:372–381. [PubMed: 16288467]

Melendez-Vasquez CV, Rios JC, Zanazzi G, Lambert S, Bretscher A, Salzer JL. Nodes of Ranvier form in association with ezrin-radixin-moesin (ERM)-positive Schwann cell processes. Proc Natl Acad Sci U S A. 2001; 98:1235–1240. [PubMed: 11158623]

Menegoz M, Gaspar P, Le BM, Galvez T, Burgaya F, Palfrey C, Ezan P, Arnos F, Girault JA. Paranodin, a glycoprotein of neuronal paranodal membranes. Neuron. 1997; 19:319–331. [PubMed: 9292722]

Peters A. The effects of normal aging on myelinated nerve fibers in monkey central nervous system. Front Neuroanat. 2009; 3:11. [PubMed: 19636385]

Peters, A.; Palay, SL.; Def, WH. The Cellular Sheaths of Neurons in the Fine Structure of the Nervous System: The Neurons and Supporting Cells. W. B. Saunders; Philadelphia: 1991.

Peters A, Sethares C. Aging and the myelinated fibers in prefrontal cortex and corpus callosum of the monkey. J Comp Neurol. 2002; 442:277–291. [PubMed: 11774342]

Peters A, Sethares C, Killiany RJ. Effects of age on the thickness of myelin sheaths in monkey primary visual cortex. J Comp Neurol. 2001; 435:241–248. [PubMed: 11391644]

Pillai AM, Thaxton C, Pribisko AL, Cheng JG, Dupree JL, Bhat MA. Spatiotemporal ablation of myelinating glia-specific neurofascin (Nfasc NF155) in mice reveals gradual loss of paranodal axoglial junctions and concomitant disorganization of axonal domains. J Neurosci Res. 2009; 87:1773–1793. [PubMed: 19185024]

Pillai AM, Garcia-Fresco GP, Sousa AD, Dupree JL, Philpot BD, Bhat MA. No effect of genetic deletion of contactin-associated protein (CASPR) on axonal orientation and synaptic plasticity. J Neurosci Res. 2007; 85:2318–2331. [PubMed: 17549747]

Pomicter AD, Shroff SM, Fuss B, Sato-Bigbee C, Brophy PJ, Rasband MN, Bhat MA, Dupree JL. Novel forms of neurofascin 155 in the central nervous system: alterations in paranodal disruption models and multiple sclerosis. Brain. 2010; 133:389–405. [PubMed: 20129933]

Rasband MN. It's "juxta" potassium channel! J Neurosci Res. 2004; 76:749–757. [PubMed: 15160387]

Rios JC, Melendez-Vasquez CV, Einheber S, Lustig M, Grumet M, Hemperly J, Peles E, Salzer JL. Contactin-associated protein (Caspr) and contraction form a complex that is targeted to the paranodal junctions during myelination. J Neurosci. 2000; 20:8354–8364. [PubMed: 11069942]

Ritchie JM, Chiu SY. Distribution of sodium and potassium channels in mammalian myelinated nerve. Adv Neurol. 1981; 31:313–328. [PubMed: 6275669]

Robertson A, Day B, Pollock M, Collier P. The neuropathy of elderly mice. Acta Neuropathol. 1993; 86:163–171. [PubMed: 7692694]

Rosenbluth J, Dupree JL, Popko B. Nodal sodium channel domain integrity depends on the conformation of the paranodal junction, not on the presence of transverse bands. Glia. 2003; 41:318–325. [PubMed: 12528185]

Rydmark M. Nodal axon diameter correlates linearly with internodal axon diameter in spinal roots of the cat. Neurosci Lett. 1981; 17:247–250. [PubMed: 7279292]

Sandell JH, Peters A. Disrupted myelin and axon loss in the anterior commissure of the aged rhesus monkey. J Comp Neurol. 2003; 466:14–30. [PubMed: 14515238]

Schafer DP, Bansal R, Hedstrom KL, Pfeiffer SE, Rasband MN. Does paranode formation and maintenance require partitioning of neurofascin 155 into lipid rafts? J Neurosci. 2004; 24:3176–3185. [PubMed: 15056697]

Schnapp B, Peracchia C, Mugnaini E. The paranodal axo-glial junction in the central nervous system studied with thin sections and freeze-fracture. Neuroscience. 1976; 1:181–190. [PubMed: 11370229]

Sherman DL, Tait S, Melrose S, Johnson R, Zonta B, Court FA, Macklin WB, Meek S, Smith AJ, Cottrell DF, Brophy PJ. Neurofascins are required to establish axonal domains for saltatory conduction. Neuron. 2005; 48:737–742. [PubMed: 16337912]

Shroff SM, Pomicter AD, Chow WN, Fox MA, Colello RJ, Henderson SC, Dupree JL. Adult CST-null mice maintain an increased number of oligodendrocytes. J Neurosci Res. 2009; 87:3403–3414. [PubMed: 19224580]

Sugiyama I, Tanaka K, Akita M, Yoshida K, Kawase T, Asou H. Ultrastructural analysis of the paranodal junction of myelinated fibers in 31 month old-rats. J Neurosci Res. 2002; 70:309–317. [PubMed: 12391590]

Suzuki K, Andrews JM, Waltz JM, Terry RD. Ultrastructural studies of multiple sclerosis. Lab Invest. 1969; 20:444–454. [PubMed: 5767418]

Swärd C, Berthold CH, Nilsson-Remahl I, Rydmark M. Axonal constriction at Ranvier's node increases during development. Neurosci Lett. 1995; 190:159–162. [PubMed: 7637883]

Tait S, Gunn-Moore F, Collinson JM, Huang J, Lubetzki C, Pedraza L, Sherman DL, Colman DR, Brophy PJ. An oligodendrocyte cell adhesion molecule at the site of assembly of the paranodal axo-glial junction. J Cell Biol. 2000; 150:657–666. [PubMed: 10931875]

Tao-Cheng JH, Rosenbluth J. Development of nodal and paranodal membrane specializations in amphibian peripheral nerves. Brain Res. 1982; 255:577–594. [PubMed: 6978754]

Tao-Cheng JH, Rosenbluth J. Axolemmal differentiation in myelinated fibers of rat peripheral nerves. Brain Res. 1983; 285:251–263. [PubMed: 6627022]

Thaxton C, Pillai AM, Pribisko AL, Labasque M, Dupree JL, Faivre-Sarrailh C, Bhat MA. In vivo deletion of immunoglobulin domains 5 and 6 in neurofascin (nfasc) reveals domain-specific requirements in myelinated axons. J Neurosci. 2010; 30:4868–4876. [PubMed: 20371806]

Vabnick I, Trimmer JS, Schwarz TL, Levinson SR, Risal D, Shrager P. Dynamic potassium channel distributions during axonal development prevent aberrant firing patterns. J Neurosci. 1999; 19:747–758. [PubMed: 9880595]

Wasserman JK, Schlichter LC. White matter injury in young and aged rats after intracerebral hemorrhage. Exp Neurol. 2008; 214:266–275. [PubMed: 18848934]

Wolswijk G, Balesar R. Changes in the expression and localization of the paranodal protein Caspr on axons in chronic multiple sclerosis. Brain. 2003; 126:1638–1649. [PubMed: 12805111]

Zhang Y, Du AT, Hayasaka S, Jahng GH, Hlavin J, Zhan W, Weiner MW, Schuff N. Patterns of age-related water diffusion changes in human brain by concordance and discordance analysis. Neurobiol Aging. 2008 epub ahead of print. 10.1016/j.neurobiolaging,2008.10.009

Zonta B, Tait S, Melrose S, Anderson H, Harroch S, Higginson J, Sherman DL, Brophy PJ. Glial and neuronal isoforms of Neurofascin have distinct roles in the assembly of nodes of Ranvier in the central nervous system. J Cell Biol. 2008; 181:1169–1177. [PubMed: 18573915]
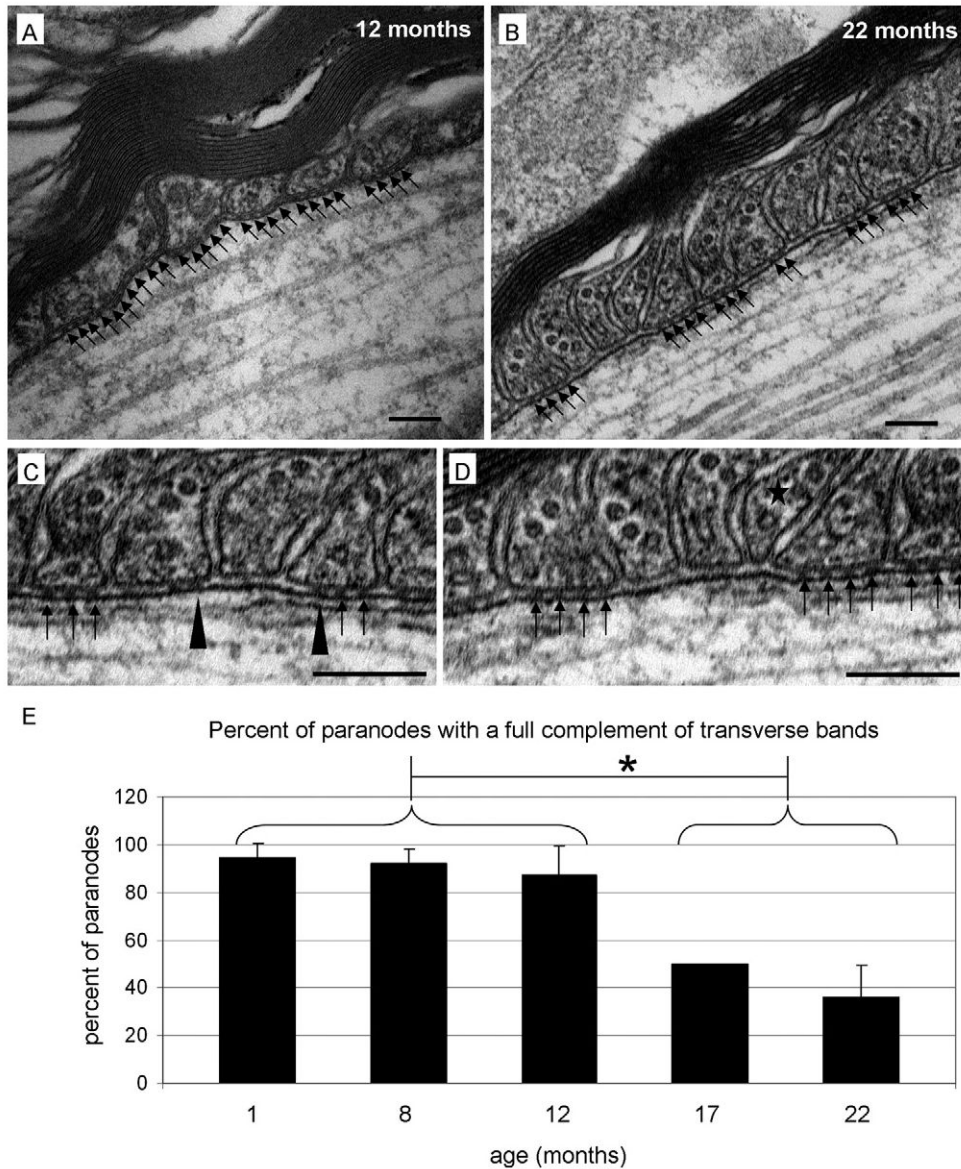
Fig. 1.
Transverse bands are reduced in aged mice. In adult (A) and aged (B) mice, paranodal loops maintain proper orientation and a close association with adjacent paranodal loops. Note the conserved width of the periaxonal space in both the adult and aged tissues. Whereas the paranodal region from the adult maintains the full complement of transverse bands (black arrows), the paranode from the aged animal contains extended lengths of periaxonal space that lack these structures (regions of periaxonal space between clusters of black arrows). High magnification images of the aged tissue clearly reveals the absence of transverse bands (C and D). In Panel C, note the transverse bands with poorly defined edges (black arrowheads), which is consistent with band deterioration. In Panel D, note the paranodal loop (star) with a reduced base, which is consistent with a loop losing its anchorage and preparing to retract. (E) Quantitative analysis revealed that transverse bands were missing at all ages; however, in mice aged 1, 8 and 12 months, the percentage of paranodes with full complement of transverse bands was approximately 90%. In contrast, 17- and 22-month-old

mice revealed a significant decrease in the percentage of paranodes exhibiting the full complement of transverse bands. $p < 0.05$; scale bars = 100 nm.
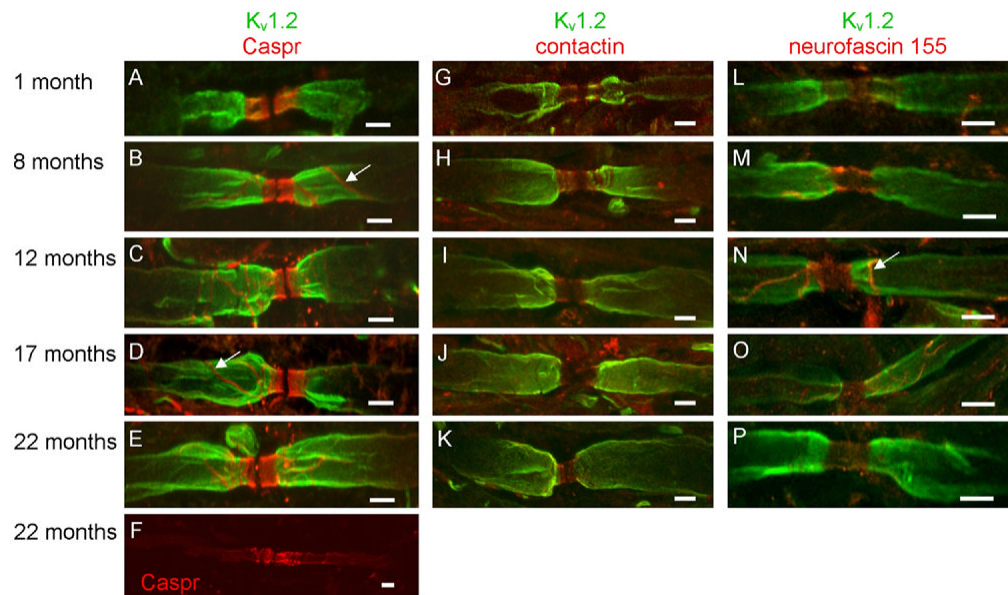
Fig. 2.
Paranodal protein domains are modestly altered in aged mice. In 1-month-old mice, Caspr (red) was restricted to the paranodal region (A). In 8- (B), 12- (C) and 17- (D) month-old mice, Caspr was observed outside the paranode; however, at these ages, extra-paranodal localization of Caspr was confined to the presumptive mesaxon (white arrows in B and D). In contrast, diffuse localization of Caspr was observed in juxtaparanodal and internodal regions of 22-month-old mice (F). In slight contrast with Caspr, contactin distribution was confined to the paranode (G–K). Similar to Caspr, neurofascin 155 was observed in all paranodal domains at all ages analyzed (L–P) and a line of immunoreactivity reminiscent of the presumed mesaxon labeled by the Caspr antibody was also observed in the anti-neurofascin labeled myelinated axons (white arrow in N). Note that $K_v1.2$ labeling (green) was occasionally observed in the paranode of young mice (G and L) but was confined to the juxtaparanode in adult and aged animals (H–K; M-P). Scale bars = 5 μm.
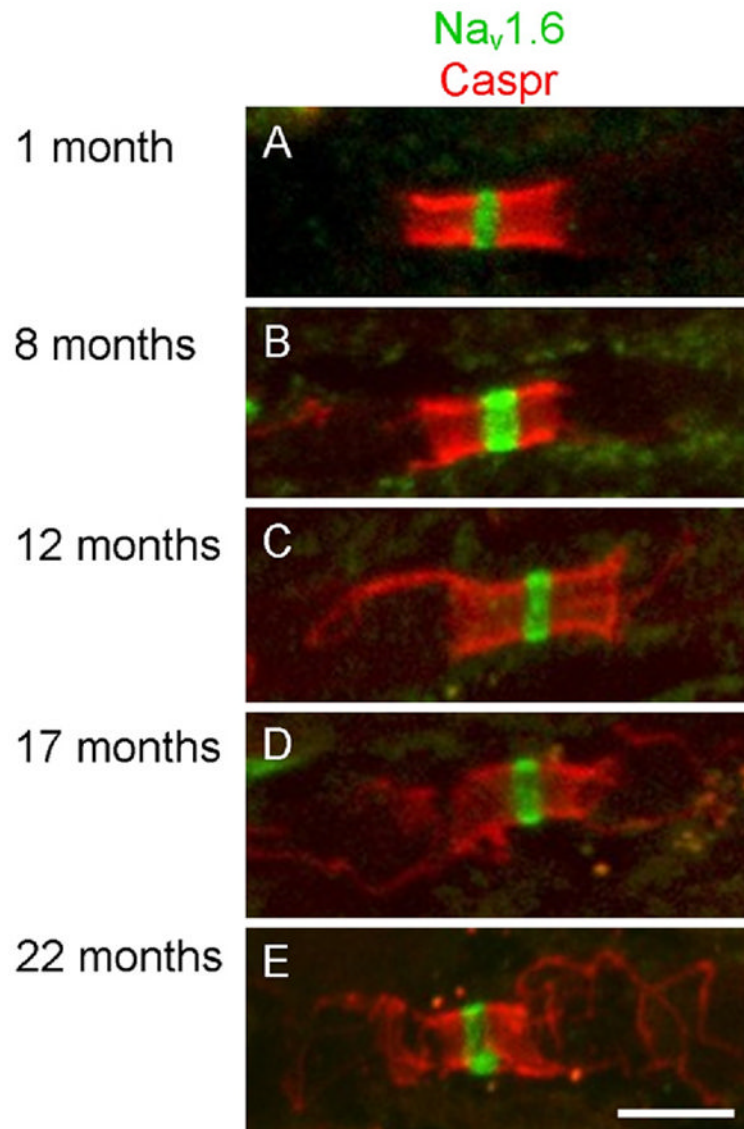
Fig. 3.
Voltage gated sodium channels were restricted to the node of Ranvier at all ages. In 1- (A), 8- (B), 12- (C), 17- (D) and 22- (E) month-old mice, clusters of $Na_v1.6$ channels (green) were restricted to the node of Ranvier. Caspr labeling (red) was used to confirm localization of the node of Ranvier. Scale bar = 5 μm.
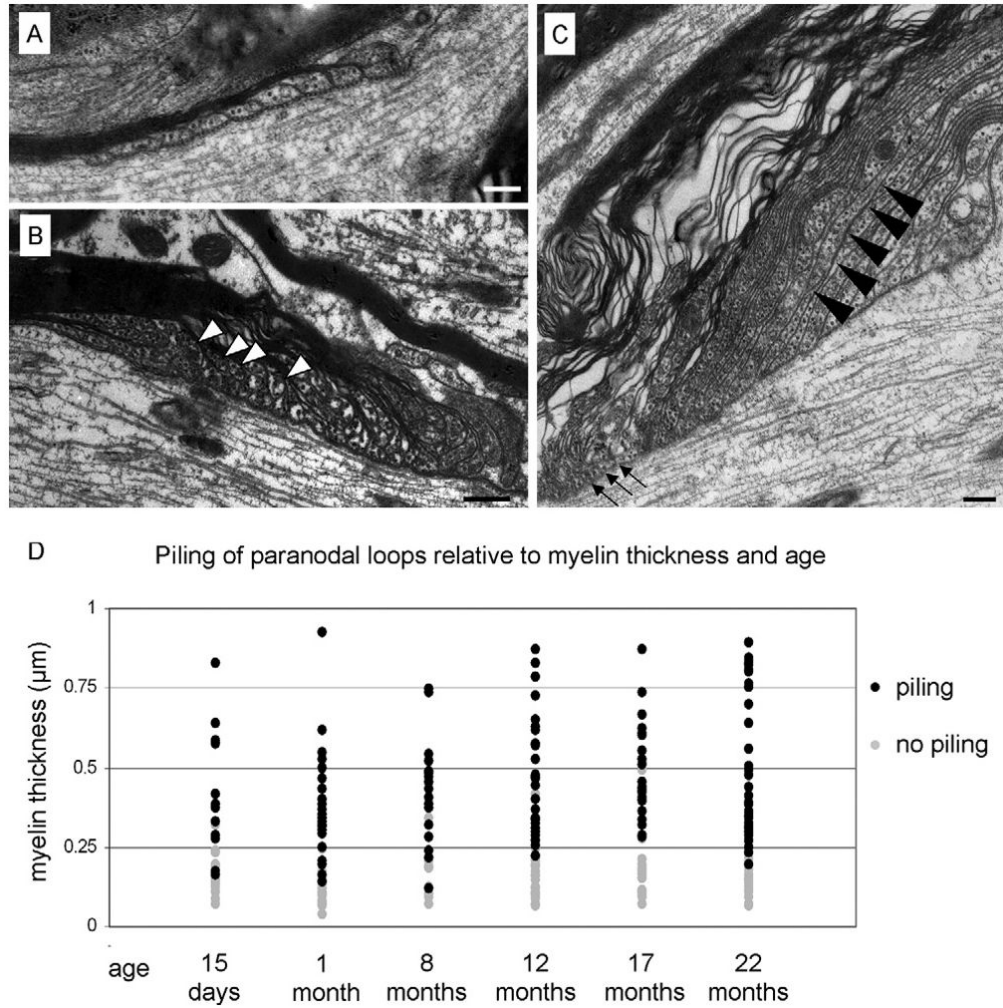
Fig. 4.
Paranodal loops "pile up" and narrow in thick myelin sheaths. Panel A displays the paranodal region of a thinly myelinated axon. The paranodal loops are of uniform width and are regularly arranged with each loop establishing contact with the axolemma. Panel B presents a paranodal region from a thick myelin sheath from a 1-month-old mouse. Note that the arrangement of the paranodal loops is irregular with centrally positioned paranodal loops (white arrowheads) piling up and not making contact with the axolemma. (C) In addition to not making contact with the axolemma, many of the paranodal loops are elongated and narrowed (black arrowheads) while many of the myelin lamellae near the node contain little or no cytoplasm (arrows). (D) Paranodes formed by myelin sheaths < 0.25 μm thick rarely exhibited piled paranodal loops. In contrast, paranodes formed by myelin sheaths ≥ 0.25 μm nearly always contained piled paranodal loops. Note that piling of paranodal loops is coincidental with myelin thickness and independent of age. Scale bars = 200 nm.
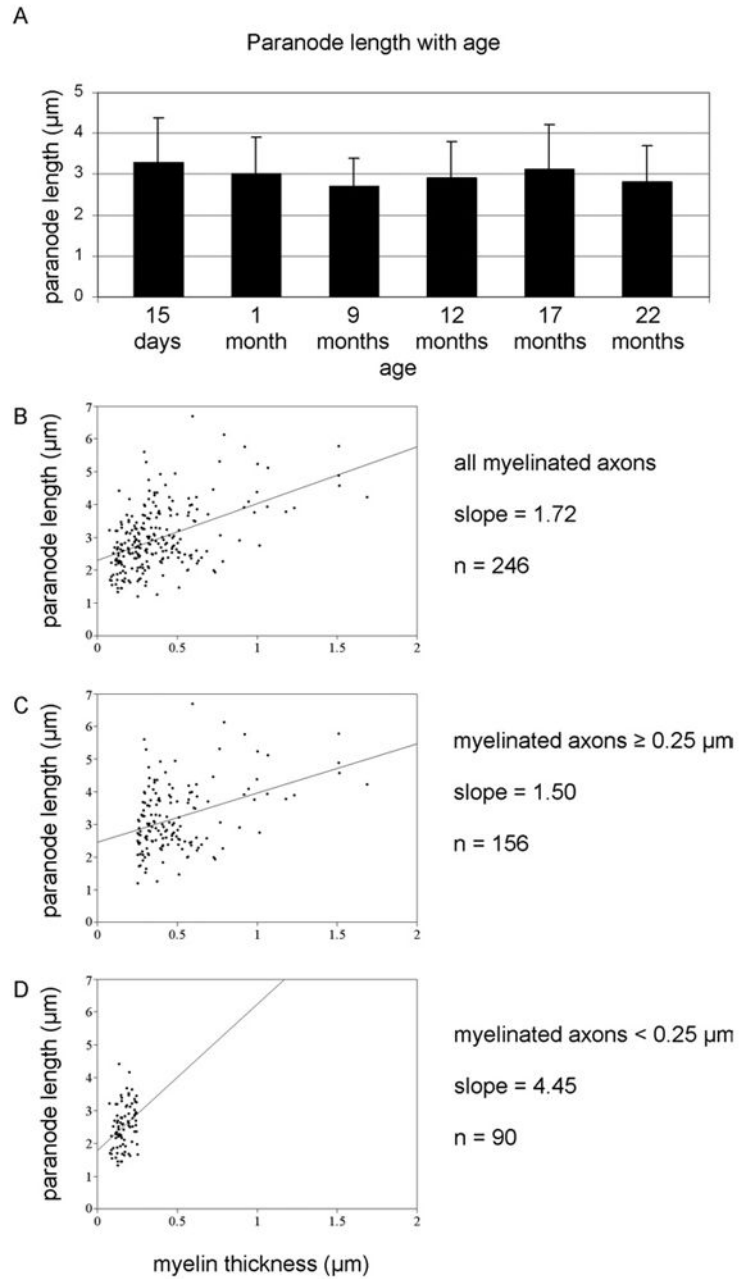
Fig. 5.
Paranodal length is conserved in the CNS. A) Mean paranodal length was not significantly different among the ages analyzed. B) A scatter plot of paranode length versus myelin thickness indicated that thicker myelin sheaths generally formed longer paranodal regions; however, the plot also indicates that the rate of paranodal lengthening is not maintained as myelin thickness increases. This difference in rate lengthening is demonstrated by graphing paranodes from myelin sheaths ≥ 0.25 um (C) separately from paranodes from myelin sheaths thinner than $0.25~\mu m$ (D). By calculating the best fit line for the two populations of paranodes, the rate of paranodal lengthening for thin sheaths was determined to be three times greater than the lengthening rate of thick sheaths.
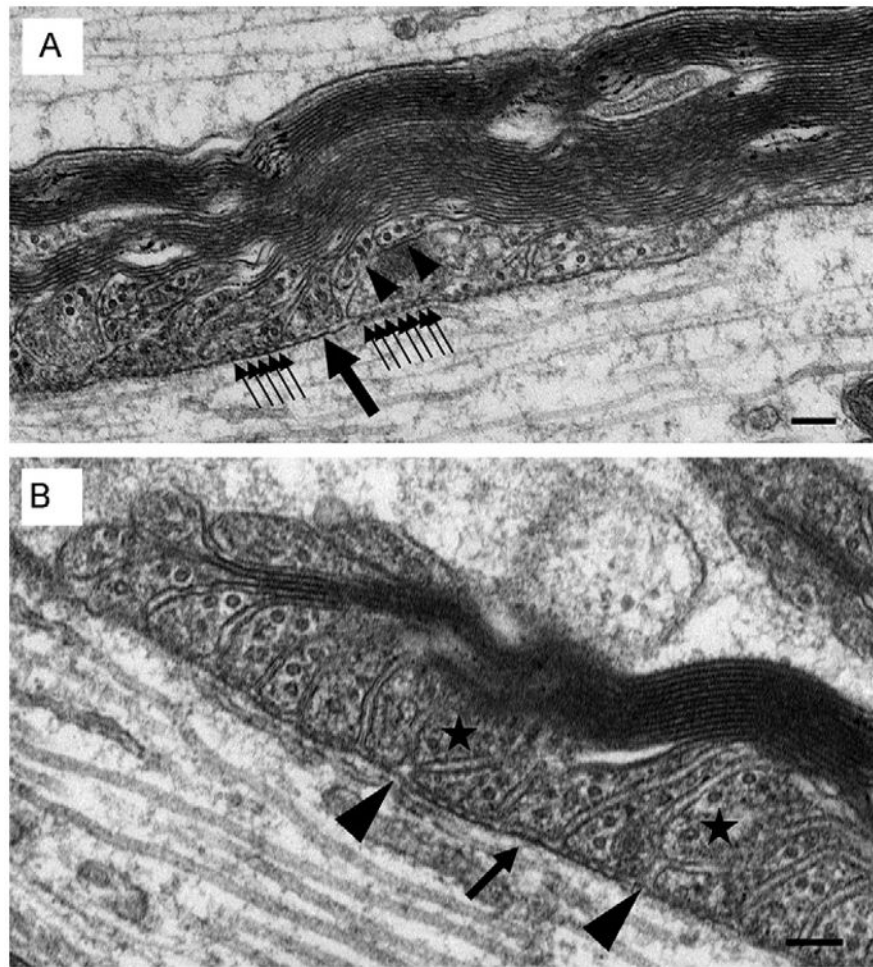
Fig. 6.
Piling of paranodal loops may result from transverse band deterioration and loop retraction. As suggested by Figure 4A, in thin myelin sheaths all paranodal loops establish contact with the axolemma and form transverse bands. A) We propose that as myelin sheaths thicken, paranodal loops (black arrowheads) lose their transverse bands and retract from the axolemma. Consistent with paranodal remodeling, note the gap left between the newly juxtaposed paranodal loops. Presumably, this gap will be filled by the repositioning of the neighboring paranodal loops. Consistent with loop repositioning, note that one of these loops (large single black arrow) lacks transverse bands while other neighboring loops exhibit the normal complement of bands (small clustered black arrows). Absence of the bands presumably facilitates loop realignment along the axonal membrane. B) Two paranodal loops have lost contact with the axolemma (stars). Note the slight gaps (black arrowheads) that remain between the newly juxtaposed paranodal loops consistent with incomplete paranodal remodeling. Scale bars = 100 nm.